PalArch's Journal of Archaeology of Egypt / Egyptology

DESIGN AND AERODYNAMIC ANALYSIS OF AN UNMANNED AERIAL VEHICLE WITH A FIXED-WING

Diego Armando Mejía Bugallo[1], Cristhian Ivan Riaño Jaimes[2], Albert Miyer Suarez Castrillon[3], Sir-Alexci Suarez Castrillon[4]

[1, 2, 3] Faculty of Engineering and Architecture, University of Pamplona, Pamplona, Colombia

[4] Faculty of Engineering, University Francisco of Paula Santander Ocaña, Colombia

ABSTRACT

This article presents the design, analysis, and simulations of a fixed-wing unmanned aerial vehicle to be used in aerial photographic captures of agricultural plantations located in the north of Colombia. In the design, the region's variable weather conditions, aerodynamic selection, lift aspects, flight efficiency, aerodynamic performance, propulsion system, and prototype structure adjusted for the application are taken into account. The design factors, requirements, and manufacture of the prototype are detailed. In the analysis and study, computational tools such as webfoil from the University of Michigan, the 3D modeling program SolidWorks 2020, the XFLR5 aerodynamic software based on xfoil with code modifications, CFD (Computational Fluid Dynamics), SolidWorks Flow Simulation, and ANSYS are used. With the results obtained, the CAD prototype of the vehicle is designed, which satisfies the calculated aerodynamic parameters. Taking into account the viability of software, it was possible to conclude that the XFLR5 ignores viscous effects; in contrast, the SolidWorks Flow Simulation CFD complement uses more elaborate equations to consider viscosity characteristics turbulence effects, in addition, the calculation methods are different while one uses the panel method the other uses Navier-Stokes equations with finite numerical methods.

INTRODUCTION

Pamplona is a Colombian municipality located in the department of Norte de Santander, located at coordinate's 72°39' longitude west of Greenwich and 7°23' north latitude. It is located at 2,200 meters above sea level, and its atmospheric pressure is 542 mmHg. Pamplona is a municipality that presents a

climatological variation, attenuating the variability in factors such as wind, precipitation, and cloudiness that make the flight of a fixed-wing drone notably tricky (Riaño et al., 2021). Fixed-wing drones need considerable space and optimal weather conditions for their correct operation, which is why wind variations are considered a design factor in this research. An aerodynamic analysis seeks to conceive a model in which the drone can fully adapt to stationary flights, leveled satisfactorily.

The purpose is to design a fixed-wing drone for which an aerodynamic analysis of a fixed-wing unmanned aerial vehicle is performed. Starting from some design considerations given by the environment where it will operate, the simulation, computational tests, and analysis will define the changes applied in the redesign of the drone. An initial model of the fixed-wing drone is analyzed to observe its aerodynamic and physical characteristics using computational tools. The most critical component within the design is the geometry and dimension of its fixed-wing, for which a profile is chosen that, given the aerodynamic and climatic conditions of Pamplona, responds in the best way to the considered design requirements.

Various efforts are being made to improve the efficiency of drone flight; below are the following international and national backgrounds related to this research and unmanned aerial vehicles. Olivos (2017), in his research "Design of the aerodynamic profile of a drone" concludes that: The correct design of an aerodynamic profile directly impacts other systems and subsystems of a drone, since if the profile has high lift coefficients, it will be able to withstand a more significant amount of payload, if the profile maintains low drag coefficients, it will need less propulsion to advance, and if the profile has high coefficients of aerodynamic efficiency, it will be able to fly for a longer time consuming a less fuel. Also, a considerable thickness in the airfoil increases the mass of the wing, but an adequate thickness provides structural security to support the loads generated by the mass of the aircraft, the power system, and the payload (Olivos, 2017). The research entitled "Design, construction, and control of a drone-type aircraft" presents an aircraft capable of sustaining itself in flight through the proposed control law (Fernandez Bobadilla et al., 2016). The controller for stabilization and regulation was adequately designed and implemented in the plant, and it was shown that it correctly processes the information about the states to produce an appropriate control signal (Fernandez, Torres, & Ramirez). The investigation entitled "Determination of the drag and lift values of the wing surfaces of a fixed-wing drone," in the investigation shows that "profiles with thicknesses greater than 18% concerning the chord as the NACA 0024 (thickness concerning the chord of 24%) are not very efficient at low Reynolds values, this is because their great thickness concerning the others generates too much drag and compromises their efficiency" (Romero Huertas, 2019). Bernal and Ortiz (2007), in his master's thesis "Wing design for an unmanned aerial vehicle," concludes that "Any aerodynamic profile that meets basic aerodynamic requirements allows it to be used in any type of aircraft and turn the process the selection process guarantees that for the established mission requirements, the profile selected under this analysis will be better adapted".
Starting from the generalities, Unmanned Aircraft System (UAS) deals with an unmanned aircraft and the equipment needed to control it remotely. (UA)

Unmanned Aircraft means any aircraft that operates or is designed to operate autonomously or piloted remotely without a pilot on board. An unmanned aerial system (UAS) has three components:

- An autonomous or human-operated control system usually on land, on a ship, or another aerial platform.
- An unmanned aerial vehicle (UAV).
- A communication, command, and control system.

UAVs can range in size from those that can be hand-launched to vehicles built or adapted in proportion to conventional fixed-wing or rotary-wing Aircraft. Drones can be classified as the mobile wing, and fixed-wing, where mobile wing drones are usually quadcopters with vertical takeoffs and landings as their main advantage, while fixed-wing drones (DAF) are their excellent aerodynamic performance can travel from a few minutes to several hours (Yao et al., 2019; Zhou et al., 2020). Other less common UAVs are airships, lighter-than-air aerial vehicles with a long-range, slow flight speed, and large size, and flapping-wing UAVs, which have flexible wings inspired by birds or insects (Gupta et al., 2013; Olivos, 2017; Teli et al., 2014; Valavanis, 2014). Among the typical applications for fixed-wing drones, the literature mentions:

- Farming.
- Emergency response including SAR.
- Facilitation of communications and broadcasting.
- Transport of trim packages and bulk loads.
- Visual, spectral and thermal examination of structures.
- Exploration of places of difficult access.
- Traffic.
- Border Surveillance.
- Archaeological investigations.
- Hydrology.
- Zoology.
- Environment.
- Photography and mapping survey.

Fixed-wing drones are designed like most drones, a fuselage composed of a central body that has two planes and a single propulsion propeller; once this fixed-wing drone is in the air, the two planes generate lift that compensates the weight allowing the drone to continue in flight, we must bear in mind that each fixed-wing drone has variants in its design characteristics according to the application to be carried out (Abbott & VonDoenhoff, 2010; Romero Huertas, 2019).

The forces acting on the fixed-wing of the drone are produced due to the surface pressure distribution and the shear stress distribution. The pressure distribution acts normal to the surface, and the shear stress distribution tangentially. The total effect of the pressures and stresses on the plane's entire surface generates an aerodynamic force. Aerodynamic force can be expressed in two components called lift and drag. Uplift acts perpendicular to the relative wind, and drag is

the force parallel to the relative wind that opposes the movement of the airfoil in a flow (Olivos, 2017).

The wing profile or aerodynamic profile is the contour of a curved shape, which, when moving through the air, creates a pressure distribution capable of maintaining its lift. The determination of the geometric relationships directly influences the aerodynamic behavior of the airfoil (Bellot & Javier, 2018; Kisabo et al., 2017).

MATERIALS AND METHODS

The applied methodology follows the recommendations made in the book "General Aviation Aircraft Design" (Gudmundsson, 2014), seeking to meet the project's needs. A Quality Function Deployment (QFD) product design methodology is applied in the development of the project. In the construction of the conceptual design, the needs survey stages are covered, the project requirements are generated to translate these requirements into engineering requirements (ReVelle et al., 1998). Within the engineering requirements, it is necessary to calculate a series of values related to the shape and geometry of the airfoil.

The use of fixed-wing drones has advantages for taking aerial photographs of agriculture; however, there are barriers to overcome to develop these tasks. The process requires trained personnel to operate the drone correctly and safely. In Pamplona city, the geography is varied and the climate. The operator must continuously fly with solid winds and cope with sudden rains (the drone must have the ability to return to the take-off point in case this happens safely) (Anderson & Eberhardt, 2001). Engineering requirements help define the geometry of the airfoil that allows the required payload to be loaded and offers the slightest drag (Demir et al., 2015). The pressure distribution of the plane is calculated to know the behavior it will have in flight (Doherty et al., 2000). Fig. 1 shows the work scheme followed for the conceptual aerodynamic design of an unmanned aerial vehicle. An aerodynamic profile that meets the requirements is selected; this profile is dimensioned and used to design the fuselage (Pérez et al., 2013; Primicerio et al., 2012; Segovia Ramírez et al., 2022).

The purpose or task for the UAV is to capture aerial photographs at low altitudes that allow monitoring the rates of vegetation destined for agriculture in the city of Pamplona, north of Santander (Eisenbeiss, 2009; Sumnall et al., 2022; Yang et al., 2022). Based on the models applied for this purpose, the following requirements were defined:

- Manual Launch.
- High altitude operation mode between 60 and 160 meters high.
- Data collection area from 50 to 80 hectares.
- Cruising speed approximately 15 m/s.
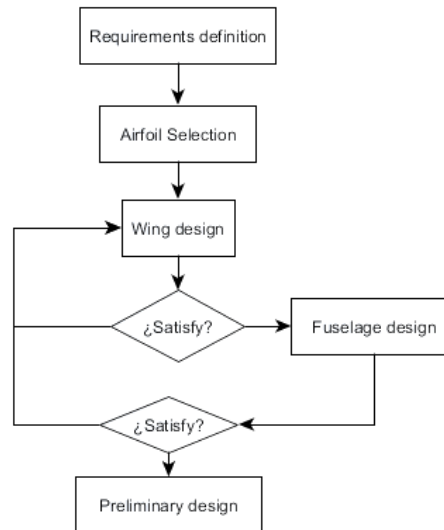- Maximum takeoff weight with equipment 2.5 kg.

Figure 1. Working scheme for aerodynamic design

The chord is the distance measured straight from the leading edge to the trailing edge. This parameter also makes it possible to determine the size and behavior of the aerodynamic profile. It is used to calculate the Reynolds number and can serve as a reference value to compare with similar purpose drone strings. The proper dimension is 0.25 m for the chord of the airfoil.

The Reynolds number is essential when preselecting airfoils since the lift coefficient depends directly on it. The airfoil pre-selection must be specific for low Reynolds numbers because most airfoils do not generate acceptable lift in these regimes. A top altitude of 60 to 160 meters and a cruising speed of 15 m/s were chosen for the calculation. The Table 1, shows the environmental variables for the city of Pamplona that were used in the modeling and simulation (Mkhitaryan, 1972).

Table 1.   The environment variables for the city

Variable	Valor
Temperature	14° [C] = 287.15 [K]
Pressure	542[mmHg] = 72260 [Pa]
The speed of sound	340.3 [m/s]
Gravitational acceleration	9.80 [m/s2]
Density	0.87 [kg/m3]

For calculating the Reynolds number (Re), equation one is used, resulting in a value of 253.14.

$$R_e = \frac{Vl}{v} \qquad\qquad (1)$$

Where
V: Cruising speed (15 m/s).
l: The proper dimension (0.25m).
v: Kinematic viscosity of air (0.01481 m²/s)
The Mach number measures the relative speed that delimits the rate at which aircraft fly in the medium they move, used to describe aircraft speed. The Mach number is determined by Equation 2, resulting in a value of 0.44.

$$M = \frac{v}{a} \qquad\qquad (2)$$

Where
v: Cruising speed (15 m/s).
a: The speed of sound (340.3m/s)

By design criterion, a profile thickness must be selected that achieves the support and structural rigidity necessary to transfer the estimated loads for the aircraft without compromising its aerodynamic behavior. It is necessary to locate the electronic elements of surveillance, navigation, and power batteries; for this, a minimum thickness of 14% is established for the chord profile. A value above this thickness increases lifts and maintains the drag and moment values.

One of the QFD methodology phases is to analyze previous works to take relevant characteristics as a reference in the design phase. This study emerged the following design requirements for the wing profile:

• Use aerodynamic profiles with geometries and dimensions close to those of fixed-wing aircraft.
• Conceive a symmetric or asymmetric profile with a high lift.
• Stable behavior for speeds between 10 to 165 km/h.

The profiles that meet the above requirements are subjected to analysis within a simulation environment, generating the necessary knowledge to establish a selection criterion for the aerodynamic profile of the wing. Table 2 summarizes the profiles considered in the study, which are evaluated according to their performance in variables such as polar drag, aerodynamic performance, and lift.

Table 2.   Profiles considered in the study phase

| Name	Classification	Name	Classification
Naca 0018	Symmetric	Naca 4415	Asymmetric
Naca 0024	Symmetric	Naca 4418	Asymmetric
Naca 0015	Symmetric	Eppler e222	Asymmetric
Avistar	Asymmetric	Naca 23018	Asymmetric
S8036	Asymmetric	Eppler 473	Symmetric
Eppler 479	Symmetric	Goe256	Asymmetric
Eppler 169	Symmetric	Naca 2415	Asymmetric
Gemini	Asymmetric	Naca 632015	Asymmetric
Naca 32015	Asymmetric		

Drag polar
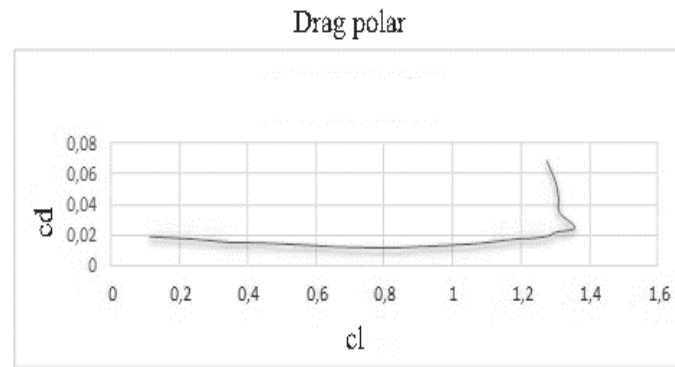
Figure 2. Polar drag curve.

The polar drag is a factor that relates the drag coefficients and the lift coefficient, where the profile that performs best is the one that has the lowest values of Cd along the graph presented in Fig. 2 and 3; it allows us to infer optimal working points. In the Cd vs. α graph, the drag coefficient increases as the angle of attack increases, it is a lower value than the lift, and care should be taken to keep the drag curve as small as possible.

The aerodynamic performance is a factor that relates the lift given by the airfoil to the amount of drag generated Cl\Cd vs. α. It is analyzed for all angles, and the highest values in the attack graph are sought to determine the best efficiency or aerodynamic performance. The angles of attack taken for the analysis range from -3° to 15° with a variation is of 0.5. The projected working angles for the UAV are between 0° to 12°. Aerodynamic efficiency is defined as lift over drag, in the Cl\Cd graph vs. α shows the efficiency for each angle. The highest value on this graph symbolizes the cruising angle, that is, the angle at which the aircraft travels with the least drag and the most lift.
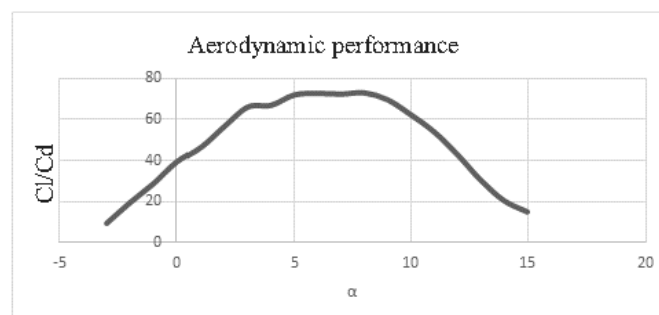

Figure 3.   Aerodynamic performance curve.

The lift force is the predominant force that relates the lift coefficient (Cl) to the angle of attack α. In Fig. 4, it can be seen that as the angle of attack increases, so does the airfoil lift. The higher the values of this graph, the better lift the profile will have. It is necessary to select an angle of attack so that the drone has a maximum L/D ratio, interpreted as the cruising angle where the most significant lift and the least drag occur. These conditions are necessary for the projected drone to fly in the established operating conditions.
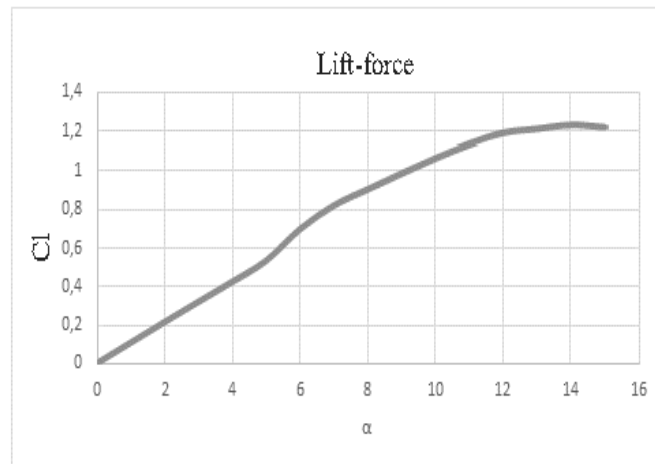
Figure 4.   Lift-force curve.

The graph Cl vs. α represents the change in lift force concerning the angle of attack; the increase is expected to be linear until it reaches a certain stall angle. The maximum lift value is found at this angle; the value obtained for this angle must not be exceeded, the lift drops off abruptly due to the detachment of the fluid from the walls of the airfoil. This value is a design criterion between different airfoils to select the airfoil that provides the most significant lift.

Fig. 5 shows the symmetric Eppler 479 airfoil. Fig. 6 shows the performance graphs for each design factor for the Eppler 479 airfoil. It can be seen from the graph that no lift is generated at an angle of attack of 0°. Aerodynamic efficiency occurs at 12°; this is due to the exponential growth of the drag curve from 12° onwards; it increases concerning lower angles, which leads to a drastic reduction in aerodynamic efficiency for higher angles.
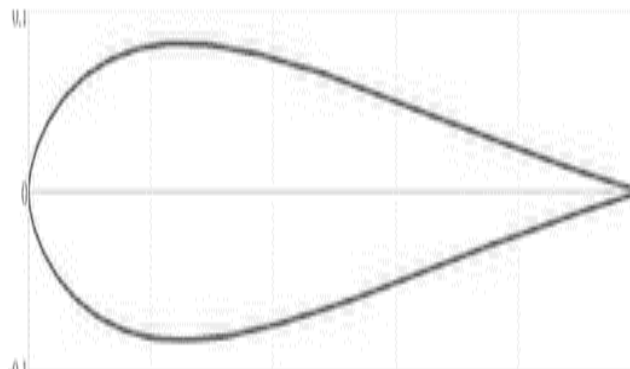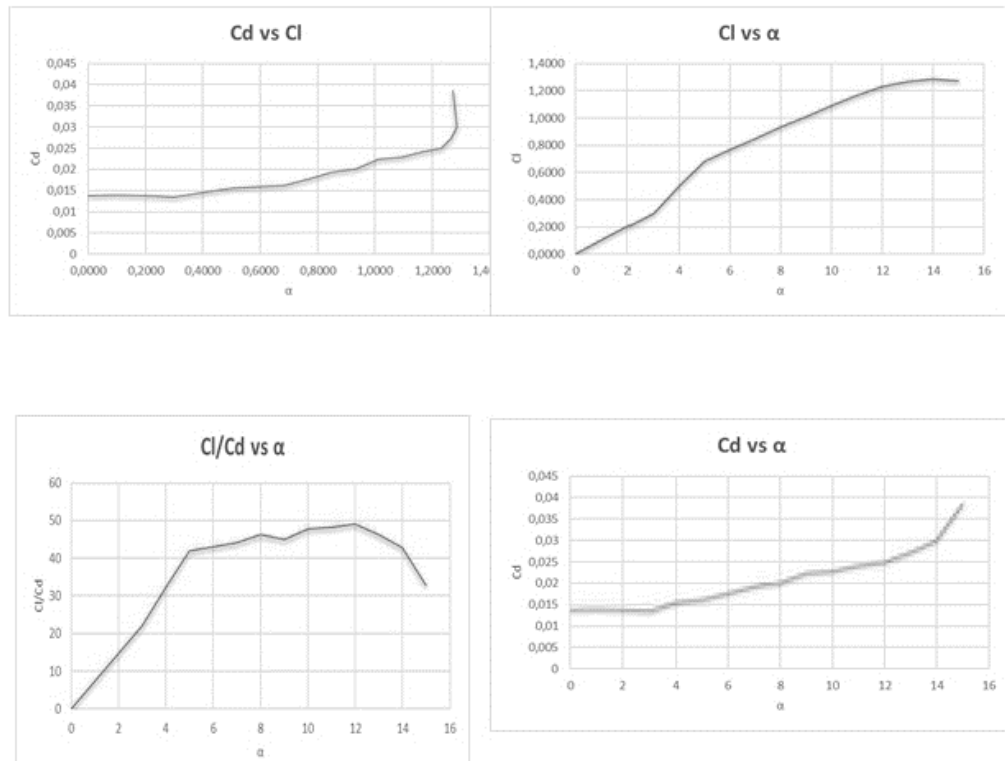

Figure 5.   Eppler Profile 479.

Figure 6. Eppler 479 Profile curves.

RESULTS

Error! Reference source not found. Fig. 7 shows the polar drag curve for the Eppler 473, Eppler 479, Naca 4415, Naca 4418, and Goe 256 profiles with the best performance within its three aerodynamic factors. It can be seen that the Naca 4415 profile, as well as the Naca 4418 profile, have the lowest drag values at all angles of attack. The Goe 256 profile at angles of $0°<Cl<5°$ presents very high drag values above the others, and for angles greater than $5°$ the curve is inverted.
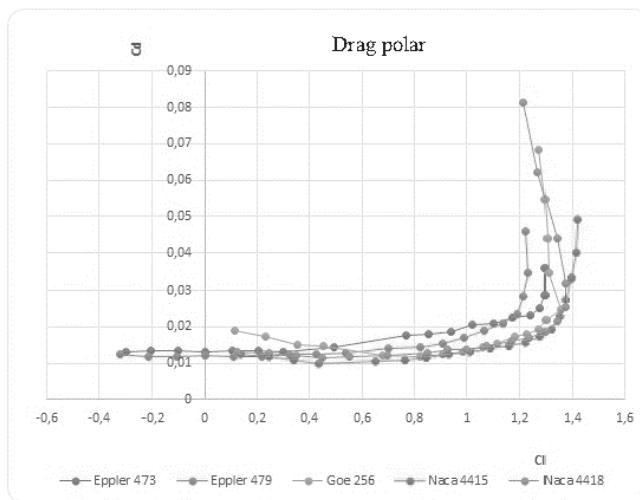

Figure 7. The polar drag curve for the Eppler 473, Eppler 479, Naca 4415, Naca 4418, and Goe 256 profiles.

The lift ratio is presented in Fig. 8, 9, and 10, and the difference between symmetrical and asymmetrical profiles can be evidenced. The relationship in a symmetric profile airfoil like the Eppler 473 and Eppler 479 have zero lift at 0° angle, while the Goe 256, Naca 4415, and Naca 4418 have around 0.44 lift.
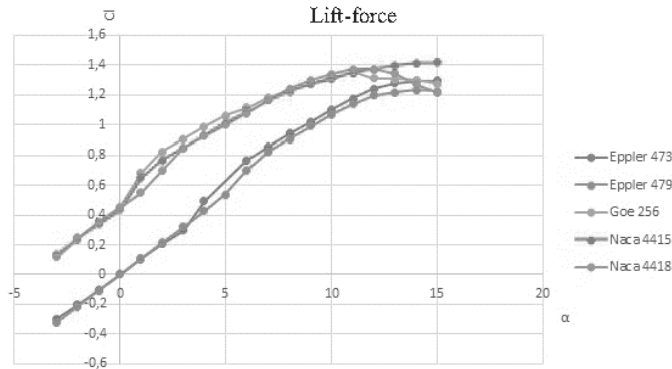

Figure 8. The lift force curve for the Eppler 473, Eppler 479, Naca 4415, Naca 4418, and Goe 256 profiles.

Table 3, maximum values of lift coefficients for each airfoil and the angle at which it appears before stalling. Presents the maximum values of lift coefficients for each airfoil and the angle at which it appears before stalling. Presents the maximum values of lift coefficients for each profile and the angle at which this value is reached. Among the airfoils with the best performance, the Naca 4415 airfoil is observed with a good lift range 0<Cl<6, as well as Goe 256, although it stalls before Naca 4418 but maintains a good Cl vs. α ratio in Cl<13. Considering the stall angle, the profiles with higher values in the graph have a better lift. The difference in maximum lift coefficients between the symmetric and asymmetric airfoils is clear.

Table 3. Maximum values of lift coefficients for each airfoil and the angle at which it appears before stalling

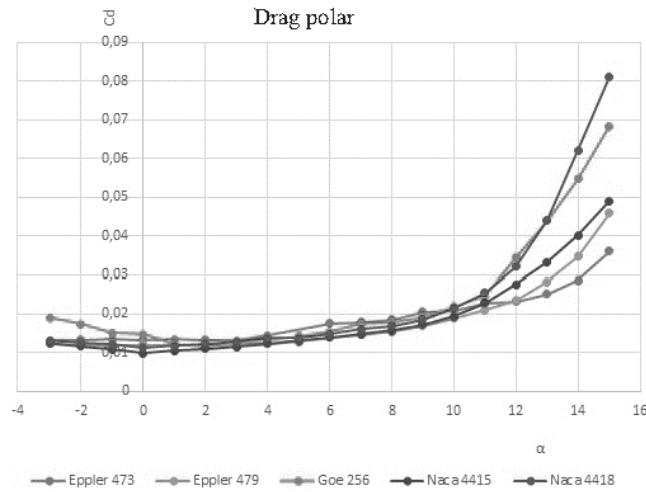| Profile Id	Cl maximum	α
Naca 4415	1.4183	15
Naca 4418	1.3744	13
Goe256	1.3558	11
Eppler 479	1.2353	14
Eppler 473	1.2479	15

Figure 9.   The drag polar curve for the Eppler 473, Eppler 479, Naca 4415, Naca 4418, and Goe 256 profiles.

Table 4.   Minimum drag coefficients 5 best profiles

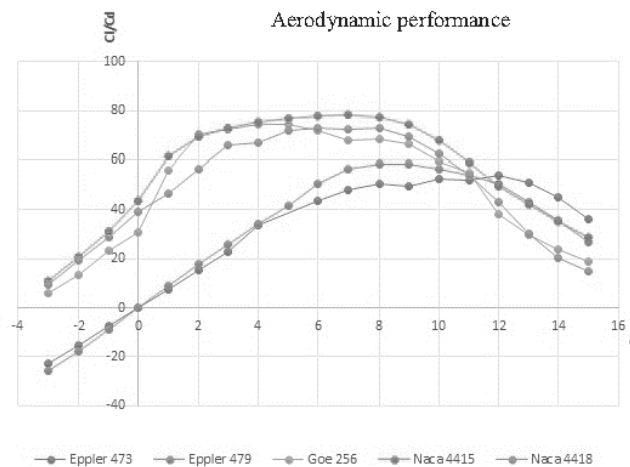| Profile Id	Cd minimum	α
Naca 4415	0.00995	0
Naca 4418	0.01143	0
Goe256	0.01169	2
Eppler 479	0.01192	1
Eppler 473	0.01309	3

Figure 10.   The aerodynamic performance curve for the Eppler 473, Eppler 479, Naca 4415, Naca 4418, and Goe 256 profiles.

Table 5. Five maximum values of aerodynamic performance for each airfoil and the angle at which it appears before stalling

Profile Id	Aerodynamic performance maximum value	optimum angle of flight
Naca 4415	78.2	7
Goe 256	74.5	5
Naca 4418	72.6	6
Eppler 479	58.2	9
Eppler 473	53.7	12

Table 3, Table 4, and Table 5, summarize the performance of the profiles in each of the curves understudies and generate a selection criterion for the profile with better lift and less drag for the UAV. The three best profiles carried out additional tests with different Reynolds numbers ranging from 253,514 to 500,000 and a Mach value of 0.04 in the subsonic regime. Fig. 11 and Fig. 12 show the resulting polar curves for the analyses applied to the previous simulation's three best profiles. The profile that stands out in this result is subsequently subjected to an analysis of simulations carried out with CFD taking into account the operating conditions in the region of the city of Pamplona. The Naca 4415 profile stands out with a more significant lift at angles greater than 7°; it also has a higher angle of attack than the other profiles studied before stalling. The aerodynamic efficiency of the Naca 4415 profile is superior to the other profiles analyzed, showing excellent lift with less drag, obtaining a better relationship between the wingspan and the necessary engine power to meet the operating requirements.
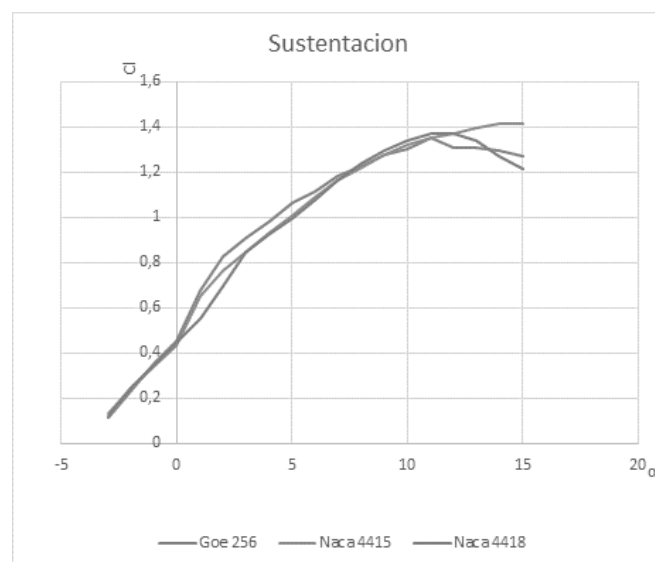

Figure 11. The lift force curve for the, Naca 4415, Naca 4418, and Goe 256 profiles.
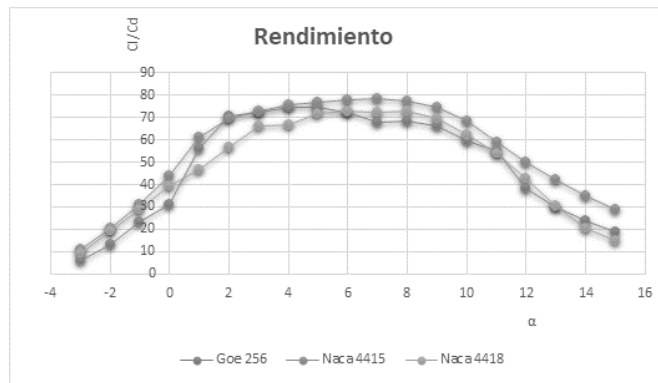
Figure 12. The aerodynamic performance curve for the, Naca 4415, Naca 4418, and Goe 256 profiles.

The profile meets the criteria selected for this project is the Naca 4415 profile. The angle of attack in the Naca 4415 profile is 7° (see Table 6**Error! Reference source not found.**); with this angle, a point with less drag is obtained while maintaining good lift, that is, a better ratio (Cl/Cd) where the highest value will be the optimum angle for a flight of the UAV.

Table 6. Drag coefficients, lift, and aerodynamic efficiency of the Naca 4415 airfoil at different angles of attack.

Profile Naca 4415				Profile Naca 4415			
α	Cl	Cd	Cl/Cd	α	Cl	Cd	Cl/Cd
-3	0.1362	0.01253	10.8699122	7	1.1624	0.01486	78.2234186
-2	0.2427	0.01170	20.7435897	8	1.2233	0.01582	77.3261694
-1	0.3382	0.01088	31.0845588	9	1.2773	0.01719	74.3048284
0	0.4348	0.00995	43.6984925	10	1.3193	0.01937	68.1104801
1	0.6497	0.01058	61.4083176	11	1.3496	0.02281	59.167032
2	0.7647	0.01099	69.5814377	12	1.3729	0.02757	49.7968807
3	0.847	0.01160	73.0172414	13	1.3954	0.03320	42.0301205
4	0.9306	0.01232	75.5357143	14	1.4123	0.04018	35.149328
5	1.0116	0.01314	76.9863014	15	1.4183	0.04901	28.938992
6	1.0887	0.01396	77.987106				

Wingspan, defined as the distance between the two wingtips of an aircraft when fully extended, is determined from the Equation (3).

$$C_l = \frac{L}{\frac{1}{2}\rho \cdot V^2 \cdot b \cdot c} \qquad (3)$$

Where
L: Lift force.
V: Speed
ρ: Fluid density.
c: Rope.
b: Envergadura.
W: Aircraft weight.

627

Where L is the lift force, ρ the fluid density, c the rope, and V the velocity, are initially provided data, instead of a lift force, there is a coefficient to replace in equation (4). Solving b from the equation 3, is to get:

$$b = \frac{W}{\frac{1}{2}\rho \cdot V^2 \cdot C_l \cdot c} \qquad (4)$$

To generate a lift of 2.5 Kgf of weight and with the lift coefficient obtained, a wingspan of 1.05 m is required; previous works in consulted literature indicate approximate values for this design value, concluding that it is within the typical range.

The aerodynamic drag coefficient Equation (6) is used to determine the power required to dimension the electric motor. The motor must meet an operating speed of 15 m/s. Equation (6) removes the generated drag and replaces it with traction; the traction value is multiplied by the operating speed.

$$C_d = \frac{T}{\frac{1}{2}\rho \cdot V^2 \cdot b \cdot c} \qquad (5)$$

$$T = \frac{1}{2} \cdot \rho \cdot V^2 \cdot b \cdot c_d \qquad (6)$$

Where
T: Traction.
V: Speed
ρ: Fluid density.
c_d: Drag coefficient.
b: Envergadura.
W: Aircraft weight.

The traction value of the required traction is 0.3707 N. Equation (7) is used to calculate the power, where the required traction is multiplied by the operating speed. The value of the power required by the motor is 5.56 W.

$$P = T \cdot V \qquad (7)$$

The traction value of the required traction is 0.3707 N. Equation 7 is used to calculate the power, where the required traction is multiplied by the operating speed. The motor is selected according to the power result obtained. It considers a safety factor of 1.5, guaranteeing the correct operation in the determined operating conditions. The selected motor must meet power of 8.34 W.

Fig. 13 presents the map of fluid densities, the area with the highest density is located on the leading edge; even so, this density, presenting variability, maintains an approximate value at all points. The analysis is performed at angles of 0°, 3°, 5°, 7°, and 12°, which correspond to the cruising angle of attack.
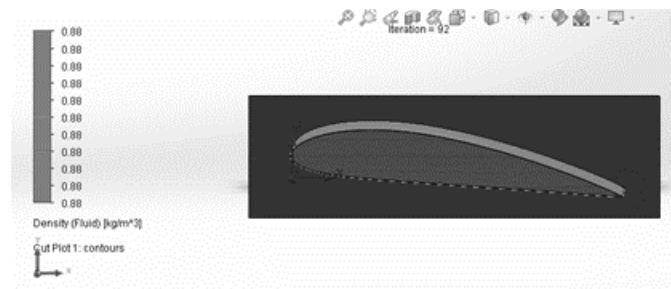
Figure 13. Flux density simulation around a Naca 4415 airfoil.

Fig. 14 shows the pressure map; the red zone indicates the zone with the highest positive pressure, and the blue zone indicates the zone with the lowest pressure, vacuum, presented in the profile. Fig. 15 shows the velocity map; it can be seen in the figure that for a determined flow velocity, an increase in local velocity is observed in the profile as a result of the geometry.
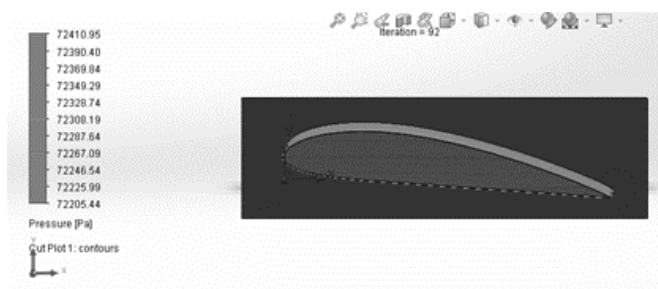

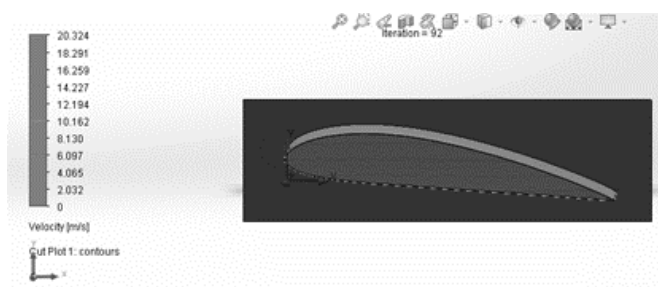**Figure 14.** Pressure simulation around a Naca 4415 airfoil.

Figure 15. Speed simulation around a Naca 4415 airfoil.

Fig. 16 shows the Mach number map. In the Mach number map, it is possible to see that both the upper and lower surfaces show the maximum Mach numbers for supersonic regimes. The SolidWorks Flow simulation CFD complement allows extracting information on the resistance forces lift of the profile, with which the aerodynamic coefficients Cl and Cd were obtained. The values of Cd are compared with those obtained in the XFLR5 software, finding excellent correspondence. The Cl values are sample differences, giving lower values in SolidWorks Flow simulation, a different product of the applied analysis methods, and the effects of additional parameters such as viscosity, fluid rotation, and turbulence. The results of the analysis performed are presented in Table 7.
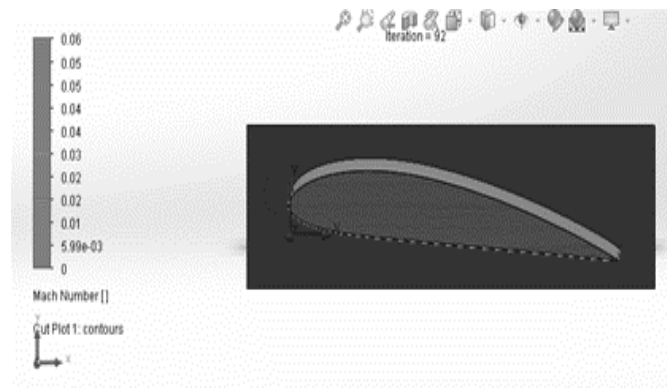
Figure 16. Mach number Naca 4415 airfoil.

Compared to the values obtained through the analytical calculations, the percentage errors of these coefficients are 31.25% and 12.37%. The calculated parameters are used for the CFD analysis of the designed wing, the calculated parameters are used, and it is also required to define simulation parameters that correspond to the established design criteria. Fig. 17 shows the design of the drone's wing, which has been tested to determine if it satisfies the flight conditions, yielding the results presented in Table V7.

Table 7.   Drag coefficients lift off the Naca 4415 airfoil at different angles of attack (Solidworks)

Naca 4415		
Angles	**Cl**	**Cd**
0°	0.1301573	0.01118147
3°	0.2995125	0.01181064
5°	0.3922308	0.02766471
7°	0.7990351	0.02424745
12°	1.2867481	0.09324589

The simulations allow inferring results to determine cruise angles and minimum angles depending on the speed of the designed application. From the simulation results obtained, a part evidenced in Fig. 17, it can be deduced that the pressure map presents an elliptical distribution and shows areas such as the front edge of the wing, where the pressure has an increased in value.
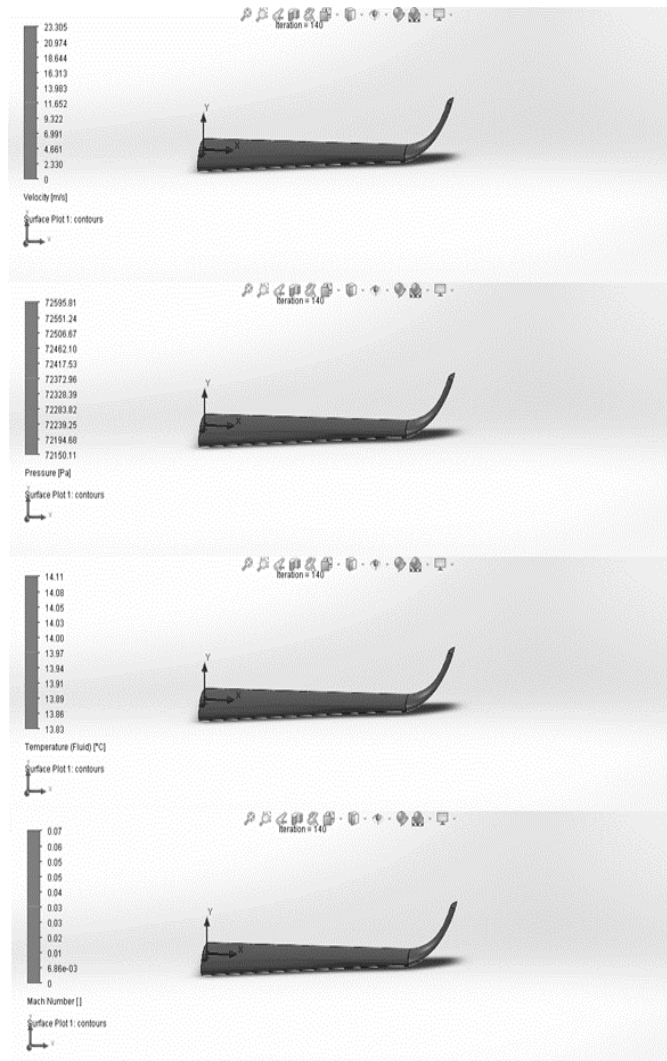
Figure 17. Modeling of the wing in speed, pressure, temperature and Mach number.

Fig. 18 illustrate the final prototype. The model was projected, designed, and developed in 3D CAD in SolidWorks, considering the design specifications, calculations, and simulation results obtained.

Table 8. Drag coefficients, wing lift at different angles of attack (Solidworks)

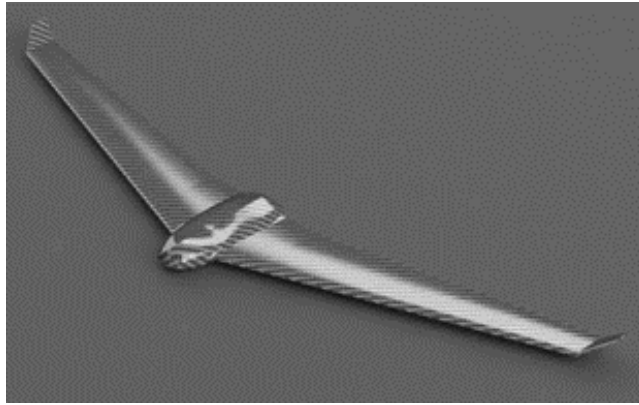| Brim with Naca 4415 profile		
Angle	Cl	Cd
0°	0.027664707	0.009623599
7°	4.989622594	0.246419418

Figure 18.   Isometric view of the virtual prototype developed from the results.

The measurements and aerodynamic parameters are adjusted to the specifications, starting from this virtual prototype to create a manufacturing and assembly engineering route to validate its simulated results in scheduled flight stages for taking aerial photographs and determining the vegetation index.

CONCLUSION
Although the analysis of an airfoil makes many assumptions that do not occur in reality, it is beneficial when beginning to design an aircraft. During the analysis of the profiles, elementary characteristics such as lift, drag, and aerodynamic efficiency are given, which are very useful in the complete planning of an aircraft.

Throughout the investigation, we concluded that every existing aerodynamic profile meets its basic requirements that allow its use in any aircraft, but not every profile is suitable for any mission; therefore, it is necessary to carry out a process of selection that guarantees compliance with the established mission requirements.

The application of aerodynamic theory requires both practical and scientific skills since a slight variation in any of the parameters involved can trigger unexpected results, in which traceability is not very viable.

According to the graphs, the CFD observed behavior adequately approximates the expected theoretical behavior.

Despite the validity of the results presented, the experimental evaluation employing a wind tunnel of a scale model of the designed wing is recommended. The collected data will guarantee the results and serve as feedback to the simulated model.

The adequate CAD modeling representing the physical aspect of the situation to be analyzed fundamental in the correct simulation of the phenomena that may occur there so that representative factors on the expected results are not omitted. CFD analyses require an iterative study and especially malicious of the available parameters offered by software manufacturers; it is necessary to understand the

impact that each of these has on the simulation so that an adequate convergence and true results are obtained with the least possible computational expense.

Although there are no cases of 2D phenomena in the physical world, the results presented have a considerable influence on the aerodynamic behavior of the 3D finite wing design.

The time available and the limited resources for the project's development are among the study's most significant limitations. Aerodynamics and CFD are very time-consuming topics to understand and properly manage.

REFERENCES

Abbott, I. H., & VonDoenhoff, A. E. (2010). *Theory of wing sections: Including a summery of airfoil data* (Unabr. and corr. republ., [Nachdr.]). Dover Publ.

Anderson, D. F., & Eberhardt, S. (2001). *Understanding flight*. McGraw-Hill.

Bellot, G., & Javier, F. (2018). *Diseño y Construcción de un Vehiculo Aereo no Tripulado Autónomo* [Proyecto/Trabajo fin de carrera/grado, Universitat Politècnica de València]. https://riunet.upv.es/handle/10251/106894

Bernal Ortiz, A., & Orrego Bustamante, S. (2007). *Diseño del ala para un vehículo aéreo no tripulado*. http://repository.eafit.edu.co/handle/10784/4450

Demir, K., Cicibaş, H., & Arica, N. (2015). Unmanned Aerial Vehicle Domain: Areas of Research. *Defence Science Journal*, *65*, 319–329. https://doi.org/10.14429/dsj.65.8631

Doherty, P., Granlund, G., Kuchcinski, K., Sandewall, E., Nordberg, K., Skarman, E., & Wiklund, J. (2000). The WITAS Unmanned Aerial Vehicle project. *Proceedings of the 14th European Conference on Artificial Intelligence*, 747–755.

Eisenbeiss, H. (2009). *A mini unmanned aerial vehicle (UAV): System overview and image acquisition*.

Fernandez Bobadilla, H. A., Torres Landín, I. J., & Ramirez Carmona, U. (2016). *Diseño, construcción y control de una aeronave tipo dron* [Universidad Nacional Autónoma de México]. https://repositorio.unam.mx/contenidos/304829

Gudmundsson, S. (2014). *General aviation aircraft design: Applied methods and procedures* (1st ed). BH, Butterworth-Heinemann/Elsevier.

Gupta, S. G., Ghonge, D. M., & Jawandhiya, P. M. (2013). *Review of Unmanned Aircraft System (UAS)* (SSRN Scholarly Paper No. 3451039). Social Science Research Network. https://doi.org/10.2139/ssrn.3451039

Kisabo, A. B., Osheku, C. A., & Samuel, S. O. (2017). Conceptual Design, Analysis and Construction of a Fixed-Wing Unmanned Arial Vehicle for Oil and Gas Pipeline Surveillance. *Journal of Aircraft and Spacecraft Technology*, *1*(1), 18–29. https://doi.org/10.3844/jastsp.2017.18.29

Mkhitaryan, A. M. (1972). *Aerodynamics*. Foreign Technology Div Wright-Patterson Afb Oh. https://apps.dtic.mil/sti/citations/AD0740190

Olivos Lara, D. (2017). *Diseño del perfil aerodinámico de un dron* [Universidad Nacional Autónoma de México]. https://repositorio.unam.mx/contenidos/251383

Pérez, M., Agüera, F., & Carvajal, F. (2013). Low cost surveying using an unmanned aerial vehicle. *The International Archives of the Photogrammetry, Remote Sensing and Spatial Information Sciences*, *XL-1-W2*, 311–315. https://doi.org/10.5194/isprsarchives-XL-1-W2-311-2013

Primicerio, J., Di Gennaro, S. F., Fiorillo, E., Genesio, L., Lugato, E., Matese, A., & Vaccari, F. P. (2012). A flexible unmanned aerial vehicle for precision agriculture. *Precision Agriculture*, *13*(4), 517–523. https://doi.org/10.1007/s11119-012-9257-6

ReVelle, J. B., Moran, J. W., & Cox, C. A. (1998). *The QFD handbook*. Wiley.

Riaño, C., Florez, E., & Peña, C. (2021). Sizing of Hybrid Photovoltaic-Wind Energy Systems Based on Local Data Acquisition. *Ingeniería y Ciencia*, *17*(33), 121–150. https://doi.org/10.17230/ingciencia.17.33.6

Romero Huertas, J. C. (2019). *Determinación de los valores de arrastre y sustentación de las superficies alares de un dron de ala fija*. https://repository.usta.edu.co/handle/11634/19483

Segovia Ramírez, I., Parra Chaparro, J. R., & García Márquez, F. P. (2022). Unmanned aerial vehicle integrated real time kinematic in infrared inspection of photovoltaic panels. *Measurement*, *188*, 110536. https://doi.org/10.1016/j.measurement.2021.110536

Sumnall, M. J., Albaugh, T. J., Carter, D. R., Cook, R. L., Hession, W. C., Campoe, O. C., Rubilar, R. A., Wynne, R. H., & Thomas, V. A. (2022). Effect of varied unmanned aerial vehicle laser scanning pulse density on accurately quantifying forest structure. *International Journal of Remote Sensing*, *43*(2), 721–750. https://doi.org/10.1080/01431161.2021.2023229

Teli, S. N., Jagtap, M., Nadekar, R., Gudade, P., More, R., & Bhagat, P. (2014). Unmanned Aerial Vehicle For Surveillance. *International Journal of Scientific & Technology Research*, *3*(5), 256–260.

Valavanis, K. P. (2014). *Handbook of unmanned*. Springer.

Yang, B., Ali, F., Zhou, B., Li, S., Yu, Y., Yang, T., Liu, X., Liang, Z., & Zhang, K. (2022). A novel approach of efficient 3D reconstruction for real scene using unmanned aerial vehicle oblique photogrammetry with five cameras. *Computers and Electrical Engineering*, *99*, 107804. https://doi.org/10.1016/j.compeleceng.2022.107804

Yao, H., Qin, R., & Chen, X. (2019). Unmanned Aerial Vehicle for Remote Sensing Applications—A Review. *Remote Sensing*, *11*(12), 1443. https://doi.org/10.3390/rs11121443

Zhou, C., Gu, S., Wen, Y., Du, Z., Xiao, C., Huang, L., & Zhu, M. (2020). The Review Unmanned Surface Vehicle Path Planning: Based on Multi-modality Constraint. *ArXiv:2007.01691 [Cs]*. http://arxiv.org/abs/2007.01691